Functional analysis of the interface between the tandem C2 domains of synaptotagmin-1

Chantell S. Evans[a,b,c], Zixuan He[a,b], Hua Bai[a,b], Xiaochu Lou[a,b], Pia Jeggle[d], R. Bryan Sutton[e], J. Michael Edwardson[d], and Edwin R. Chapman[a,b,c,*]

[a]Howard Hughes Medical Institute, [b]Department of Neuroscience, and [c]Molecular and Cellular Pharmacology Program, University of Wisconsin–Madison, Madison, WI 53705-2275; [d]Department of Pharmacology, University of Cambridge, Cambridge CB2 1PD, UK; [e]Department of Cell Physiology and Molecular Biophysics, Texas Tech University Health Sciences Center, Lubbock, TX 79430

ABSTRACT **C2 domains are widespread motifs that often serve as Ca^{2+}-binding modules; some proteins have more than one copy. An open issue is whether these domains, when duplicated within the same parent protein, interact with one another to regulate function. In the present study, we address the functional significance of interfacial residues between the tandem C2 domains of synaptotagmin (syt)-1, a Ca^{2+} sensor for neuronal exocytosis. Substitution of four residues, YHRD, at the domain interface, disrupted the interaction between the tandem C2 domains, altered the intrinsic affinity of syt-1 for Ca^{2+}, and shifted the Ca^{2+} dependency for binding to membranes and driving membrane fusion in vitro. When expressed in syt-1 knockout neurons, the YHRD mutant yielded reductions in synaptic transmission, as compared with the wild-type protein. These results indicate that physical interactions between the tandem C2 domains of syt-1 contribute to excitation–secretion coupling.**

Monitoring Editor
Patrick J. Brennwald
University of North Carolina

Received: Jul 15, 2015
Revised: Dec 12, 2015
Accepted: Jan 12, 2016

INTRODUCTION

C2 domains are conserved protein modules of ~135 residues (Nalefski and Falke, 1996). The term "C2 domain" arose from the cloning of protein kinase C (PKC) isoforms and refers to the second of four conserved motifs (motif 2) in "classical" isoforms of PKC that require anionic phospholipids and Ca^{2+} for maximal activity. These motifs are absent in "nonclassical" PKC isoforms that are not regulated by Ca^{2+} (Nishizuka, 1988; Ohno *et al.*, 1988; Ono *et al.*, 1988). Since this original work, it is now apparent that C2 domains are present in a variety of signaling and membrane-trafficking proteins, in which they mediate interactions with other molecules, including intracellular proteins and membranes, in a manner often regulated by Ca^{2+} (Nalefski and Falke, 1996).

The systematic cloning of synaptic vesicle (SV) proteins revealed that the previously characterized glycoprotein p65 (renamed synaptotagmin [syt]-1) harbored tandem C2 domains (Matthew *et al.*, 1981; Perin *et al.*, 1990), C2A and C2B, that are connected by a short linker segment. Syt-1 spans the SV membrane once and was the first integral membrane protein found to harbor C2 domains. In syt-1, both C2 domains bind Ca^{2+} via two flexible loops, 1 and 3, that protrude from the "top" of each domain (Sutton *et al.*, 1995); C2A binds three Ca^{2+} ions (Ubach *et al.*, 1998), while C2B binds two Ca^{2+} ions (Fernandez *et al.*, 2001).

Ca^{2+} promotes the interaction of syt-1 with membranes that harbor anionic phospholipids (Perin *et al.*, 1990; Brose *et al.*, 1992). Upon binding Ca^{2+}, the loops of syt-1 partially insert into the target membrane (Chapman and Davis, 1998; Bai *et al.*, 2002; Chicka *et al.*, 2008). This insertion step serves to drive the close apposition of the SV and plasma membrane (Chicka *et al.*, 2008) and might also drive

This article was published online ahead of print in MBoC in Press (http://www.molbiolcell.org/cgi/doi/10.1091/mbc.E15-07-0503) on January 20, 2016.

C.S.E., H.B., and X.L. conducted and analyzed the biochemistry experiments. Z.H. conducted and analyzed the electrophysiological experiments. P.J. and J.M.E. performed and analyzed the atomic force microscopy experiments. R.B.S. provided critical discussion and comments regarding the manuscript. C.S.E. and E.R.C. wrote the manuscript.

The authors declare no competing financial interests.

*Address correspondence to: Edwin R. Chapman (chapman@wisc.edu).

Abbreviations used: AFM, atomic force microscopy; cd-Syb, cytoplasmic domain of syb; CLM, Ca^{2+} ligand mutant; DIV, days in vitro; EPSCs, excitatory postsynaptic currents; GST, glutathione *S*-transferase; HBS, HEPES-buffered saline; ITC, isothermal titration calorimetry; KO, knockout; mEPSC, miniature excitatory postsynaptic currents; NBD-PE, 1,2-dipalmitoyl-*sn*-glycero-3-phospho-ethanolamine-*N*-(7-nitro-2-1,3-benzoxadiazol-4-yl); NMR, nuclear magnetic resonance; PBS, phosphate-buffered saline; PC, phosphatidylcholine; PE, phosphatidylethanolamine; PKC, protein kinase C; PS, phosphatidylserine; Rho-PE, *N*-(lissamine rhodamine B sulfonyl)-1,2-dipalmitoyl-*sn*-glycero-3-phosphoethanolamine; RRP, readily releasable pool; RT, room temperature; SNARE, soluble *N*-ethylmaleimide–sensitive factor attachment protein receptor; SV, synaptic vesicle; syb, synaptobrevin-2; syt-1, synaptotagmin-1; syt-3, synaptotagmin-3; syx, syntaxin-1A; Syxr, syx-only vesicles; Tr, t-SNARE heterodimer vesicles; t-SNARE, target membrane SNARE; v-SNARE, vesicular membrane SNARE; WT, wild type.

the localized buckling of the target membrane (Araç *et al.*, 2006; Martens *et al.*, 2007; Hui *et al.*, 2009), thereby facilitating fusion. Ca^{2+} also enhances the binding of syt-1 to soluble *N*-ethylmaleimide–sensitive factor attachment protein receptors (SNAREs), which form the core of a conserved membrane fusion machine. Vesicular (v-) and target (t-) membrane SNAREs assemble into four-helix bundles that directly catalyze fusion. Syt-1 specifically binds to t-SNAREs (Bennett *et al.*, 1992; Schiavo *et al.*, 1997; Davis *et al.*, 1999) and drives their assembly into heterodimers in vitro (Bhalla *et al.*, 2006; Hui *et al.*, 2011).

While the role of syt•t-SNARE interactions remains unclear in vivo (Zhang *et al.*, 2002, 2010), the interaction of syt-1 with membranes appears to be a key step in excitation–secretion coupling (Liu *et al.*, 2014). In a recent study, the length and rigidity of the linker that connects C2A and C2B was systematically varied. These alterations resulted in a graded ability of syt-1 to penetrate membranes, and these changes were well correlated with the ability of the linker mutants to drive SV exocytosis, thus uncovering a step in excitation–secretion coupling (Liu *et al.*, 2014). These experiments suggested that holding the C2 domains apart, using long polyproline rods, disrupted the function of syt-1, supporting a model in which the tandem C2 domains must cooperate to drive efficient membrane fusion. However, the notion that C2A and C2B engage in intramolecular interactions remains controversial (Sutton *et al.*, 1999; Bai *et al.*, 2002; Araç *et al.*, 2006; Fuson *et al.*, 2007; Fealey *et al.*, 2012). Hence a more subtle approach, using point mutations of interfacial residues instead of artificial linkers to disrupt contact between the tandem C2 domains, should help to inform studies of interdomain interactions.

Three crystal structures of the cytoplasmic domain of syt have been reported: one for syt-1 and two for syt-3 (Sutton *et al.*, 1999; Fuson *et al.*, 2007; Vrljic *et al.*, 2010). These structures differ in the relative orientation of the C2 domains, which might reflect different functional states of the protein. In the "open" conformation, the metal/phospholipid binding loops of each C2 domain of syt faced one another, and there were no interdomain interactions (Sutton *et al.*, 1999). However, in the "closed" state, an interdomain association was clearly apparent (Fuson *et al.*, 2007). Between these two conformations, the interfacial residues Y180 and H237 in C2A and R388 and D392 in C2B exhibited considerable differences in spatial orientation and bonding interactions (Fuson *et al.*, 2007). In the isolated syt-1 C2A structure, loop 3 was stabilized by intradomain interactions between Y180 and H237 (Fuson *et al.*, 2007). However, in the structure of the cytoplasmic domain, Fuson *et al.* (2007) found that the Y180/H237 interaction was disrupted, resulting in the distortion of loop 3 and the formation of a new interdomain interaction between H237 in C2A and T406 in C2B. This led to the idea that C2A was inactivated in the presence of C2B (Fuson *et al.*, 2007). Consistent with this idea, a number of studies reported that disruption of Ca^{2+} binding to C2A by substituting Ca^{2+} coordinating residues had little effect on synaptic transmission (Fernandez-Chacon *et al.*, 2002; Robinson *et al.*, 2002; Stevens and Sullivan, 2003). Finally, the structure by Fuson *et al.* (2007) revealed that residues R388 and D392, present in an α-helical insertion in C2B, form salt bridges with D178 and R199/233 of C2A, respectively.

In this study, we carried out experiments to determine whether disruption of the putative interaction surface between C2A and C2B by point mutations of interfacial residues, YHRD, altered the function of syt-1. As detailed below, using a combination of biophysical and biochemical approaches, in conjunction with atomic force microscopy (AFM) and electrophysiology, we observed that intramolecular interactions play an important role in syt-1 function during excitation–secretion coupling.

RESULTS

C2 domain tethering affects the intrinsic affinity of syt-1 for Ca^{2+}

To determine whether tethering C2A and C2B together, via the native linker, affects Ca^{2+}-binding activity, we carried out isothermal titration calorimetry (ITC) experiments (Figure 1A). ITC measures the changes in heat associated with the binding of a ligand

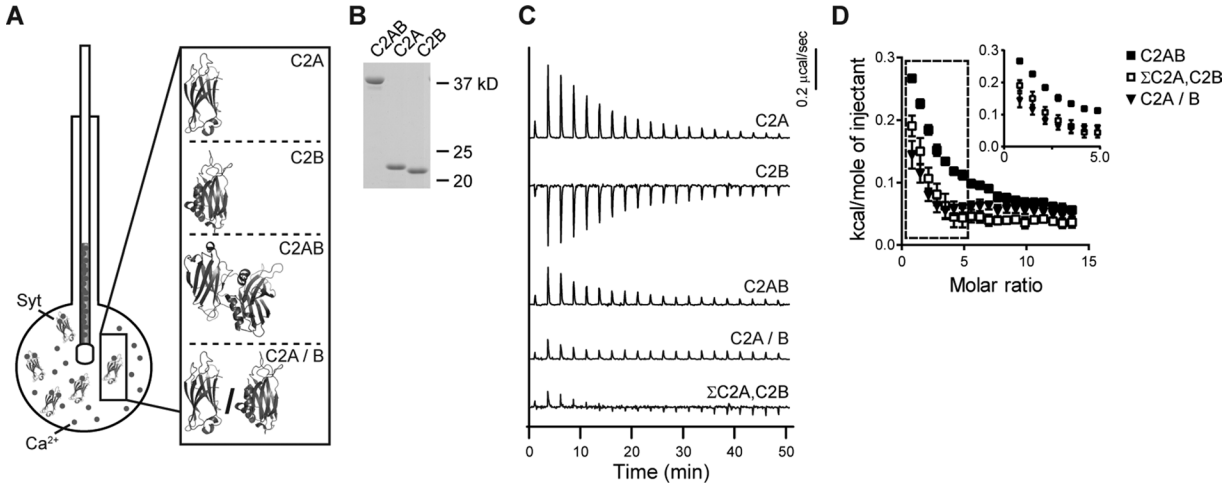

FIGURE 1: The Ca^{2+}-binding activity of syt-1 depends on tethering its tandem C2 domains together. (A) Schematic illustrating ITC experiments in which Ca^{2+} is injected into a sample cell containing fragments of syt-1 (structures from Fuson *et al.*, 2007). (B) A representative SDS–PAGE gel of the proteins (0.6 µg) used in the ITC experiments. (C) Heat of binding was measured for equal molar amounts of isolated C2A, isolated C2B, tethered C2AB, or the severed C2 domains, denoted C2A/B. For additional comparison, the traces obtained using isolated C2A and C2B were summed (ΣC2A,C2B). Shown are representative traces; $n \geq 3$. (D) Isotherms of ΣC2A,C2B and C2A/B are significantly different from tethered C2AB. The inset shows the first seven data points on an expanded scale; error bars indicate SEM. Thermodynamic values are provided in Table 1.

	K_d (μM)	ΔH (cal/mol)	ΔS (cal/mol/K)	ΔG (kcal/mol)
C2A	K_{d1} = 42.8 ± 10	ΔH_1 = 813 ± 170	ΔS_1 = 23.0 ± 0.69	ΔG_1 = –6.05 ± 0.17
	K_{d2} = 164 ± 28	ΔH_2 = 1510 ± 230	ΔS_2 = 22.6 ± 0.47	ΔG_2 = –5.21 ± 0.12
	K_{d3} = 1430 ± 230	ΔH_3 = 2430 ± 290	ΔS_3 = 21.3 ± 1.1	ΔG_3 = –3.92 ± 0.095
C2B	K_{d1} = 191 ± 35	ΔH_1 = –652 ± 130	ΔS_1 = 15.1 ± 0.86	ΔG_1 = –5.16 ± 0.17
	K_{d2} = 262 ± 18	ΔH_2 = –1590 ± 69	ΔS_2 = 11.1 ± 0.35	ΔG_2 = –4.89 ± 0.043
C2AB	K_{d1} = 26.2 ± 7.6	ΔH_1 = 304 ± 110	ΔS_1 = 22.4 ± 0.41	ΔG_1 = –6.37 ± 0.13
	K_{d2} = 186 ± 26	ΔH_2 = 577 ± 99	ΔS_2 = 19.2 ± 0.32	ΔG_2 = –5.21 ± 0.12
	K_{d3} = 300 ± 64	ΔH_3 = 520 ± 410	ΔS_3 = 18.2 ± 1.2	ΔG_3 = –4.89 ± 0.12
	K_{d4} = 1750 ± 330	ΔH_4 = 2340 ± 820	ΔS_4 = 20.7 ± 2.6	ΔG_4 = –3.83 ± 0.11

Representative traces and isotherms are shown in Figure 1. Data are presented as mean ± SEM, $n \geq 3$.

TABLE 1: ITC analysis of Ca^{2+} binding to isolated and tandem C2 domains of syt-1.

to a macromolecule of interest. Resulting heat changes are then analyzed to determine thermodynamic properties of the interaction. We turned to ITC to study interdomain interactions of syt-1, as other biophysical approaches yielded inconclusive results, as detailed in the *Introduction*. In the current study, titrations were performed using only Ca^{2+} and syt-1 fragments. Therefore the intrinsic Ca^{2+}-binding properties of syt-1, independent of other targets or effectors (i.e., membranes and t-SNAREs), were directly determined. Ca^{2+} was titrated into a sample cell containing isolated C2A; isolated C2B; or the tethered, tandem C2 domains (C2AB). We note that similar experiments were reported in a previous study (Radhakrishnan *et al.*, 2009) using relatively high [protein] and [Ca^{2+}]. Under these conditions, in our hands, aggregation of C2B and C2AB occurred (unpublished data; Damer and Creutz, 1996; Hui *et al.*, 2011), raising concerns that the heat of Ca^{2+} binding measured in the earlier experiments might be confounded by the self-association of these protein fragments. We addressed this issue by conducting ITC experiments at both high (Supplemental Figure S1 and Supplemental Table S1) and low protein concentrations (Figure 1 and Table 1). In all cases, equal molar amounts of protein were analyzed (Figure 1B and Supplemental Figure S1A). Surprisingly, similar results were obtained under both conditions, so aggregation does not appear to have a significant effect in these thermodynamic experiments.

Ca^{2+} binding to isolated C2A was endothermic, while binding of Ca^{2+} to C2B was exothermic (Figure 1C and Supplemental Figure S1, B and C), so C2AB yielded a relatively small endothermic signal due to cancellation of the heat of binding to the two C2 domains (Figure 1C and Supplemental Figure S1D). Severed C2A/B (i.e., heat of binding measured from isolated C2A and C2B together in the same sample cell) and the sum of the traces obtained from isolated C2A and isolated C2B, measured independently (denoted ΣC2A,C2B), were also analyzed for comparison; both exhibited little to no signal (Figure 1C). When fitted with a "sequential binding-site" model, C2A exhibited three binding sites with K_d values of 42.8 μM, 164 μM, and 1.4 mM; C2B had two binding sites, with K_d values of 191 μM and 262 μM. Given that the two binding sites in C2B had similar K_d values, C2AB was fitted using a four-site sequential binding-site model, resulting in K_d values of 26.2 μM, 186 μM, 300 μM, and 1.7 mM. These values are consistent with previously reported nuclear magnetic resonance (NMR) and ITC data (Ubach *et al.*, 1998; Fernandez *et al.*, 2001; Radhakrishnan *et al.*, 2009); all thermodynamic data are provided in Table 1. Signals from C2A/B and ΣC2A,C2B were too small to accurately fit.

We next compared the isotherms obtained from tethered C2AB with those for C2A/B and ΣC2A,C2B (Figure 1D). If C2A and C2B do not interact, then the sum of the isotherms obtained for these domains, in isolation, should be similar to the isotherm for C2AB. While the isotherms for C2A/B and ΣC2A,C2B were virtually identical to each other, the isotherm for C2AB was clearly different. So, while K_d values for C2A/B and ΣC2A,C2B could not be determined, qualitative comparisons demonstrate clear differences in the energetics of Ca^{2+}-binding activity as compared with the tethered C2AB. To the best of our knowledge, these data provide the first indications that the intrinsic affinity of syt-1 for Ca^{2+} is affected by the close proximity of its tandem C2 domains.

We also made use of previously characterized Ca^{2+} ligand mutant (CLM) forms of syt-1 in which three acidic Ca^{2+} ligands in each C2 domain were neutralized (Supplemental Figure S2; Chapman, 2008); for completeness, three native Asp residues were substituted with either Asn or Ala. In all cases, equal molar amounts of protein were analyzed (Supplemental Figure S2A), facilitating direct comparisons between ITC traces. As expected, when both C2 domains were mutated, no Ca^{2+}-binding activity was detected (Supplemental Figure S2, B and C).

Interestingly, we also confirmed that when Ca^{2+} binding in each C2 domain was disrupted, the ITC traces resulting from the remaining active domain were identical to those obtained using the same domain in isolation (Supplemental Figure S2, B and C, and Supplemental Table S2; Radhakrishnan *et al.*, 2009). Hence studies of severed C2 domains indicate cooperation between them in terms of sensing Ca^{2+}, while experiments using CLMs failed to reveal cooperation, a point we return to in the *Discussion*. To gain further insight into this issue, we mutated residues in the interfacial region between C2A and C2B to determine their impact on the Ca^{2+}-binding activity and function of syt-1.

Disruption of inter–C2-domain surface alters Ca^{2+} binding

It has been proposed that four residues, Y180, H237, R388, and D392, contribute to interfacial contacts between the tandem C2 domains of syt-1 (Figure 2A, residues are labeled and interdomain interactions are shown as dotted lines; Fuson *et al.*, 2007). These four residues (denoted YHRD) were mutated in wild-type (WT) C2AB; Y180 was substituted with a Phe, and the other residues (H237/R388/D392) were changed to Ala. In parallel, we also mutated these residues in a mutant form of C2AB in which the native linker that connects the tandem C2 domains was tripled (designated 3×C2AB) to facilitate analysis by AFM experiments, as detailed below; the

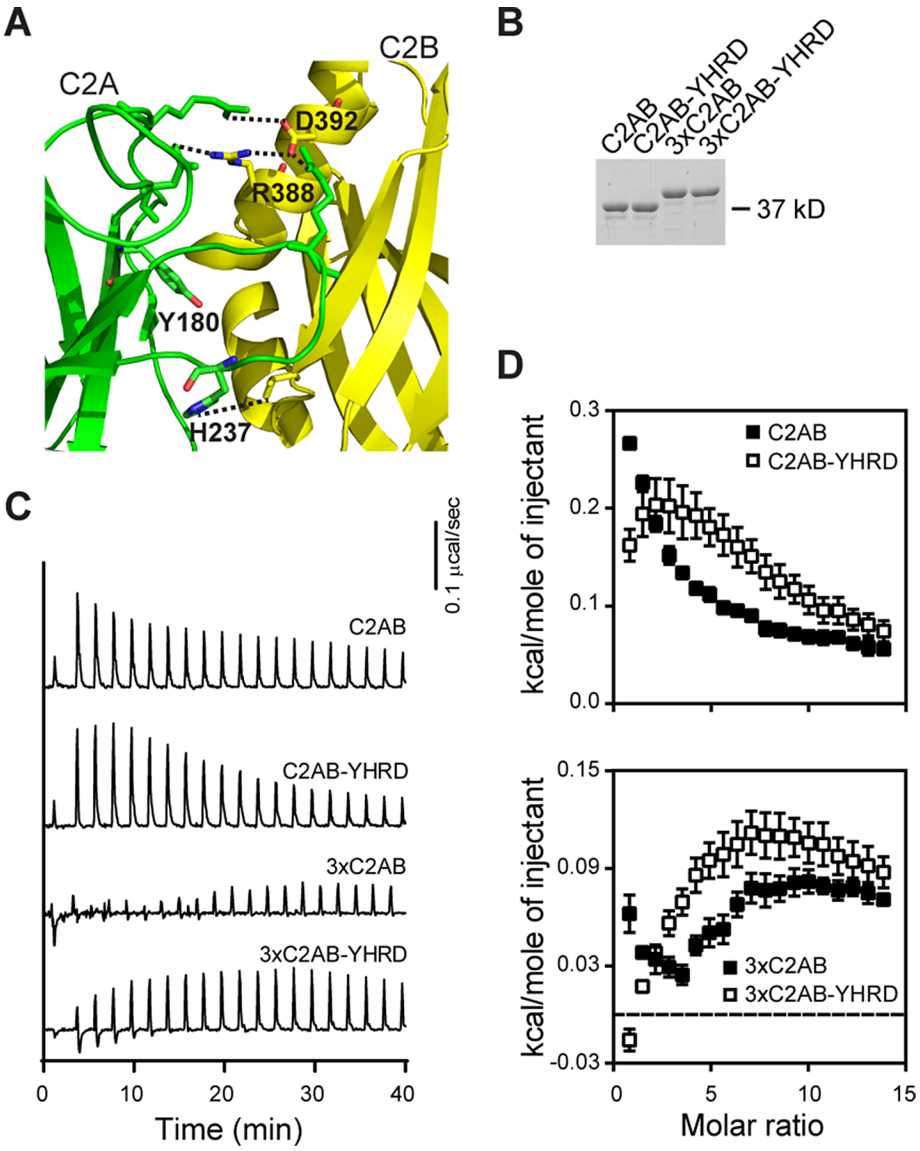

FIGURE 2: Mutations that disrupt putative inter–C2-domain interactions alter Ca^{2+} binding. (A) Structural model depicting four residues (Y180, H237, R388, and D392; interdomain interactions are shown as dotted lines) proposed to mediate interactions between the tandem C2 domains of syt-1 (C2A, green; C2B, yellow; from Figure 1A). These four residues, denoted YHRD, were mutated in a WT C2AB and a 3×C2AB mutant background. In the 3×C2AB construct, the native linker sequence between the C2A and C2B was tripled (Liu *et al.*, 2014). (B) Representative SDS–PAGE gel of the proteins (0.6 µg) used in the ITC experiments. (C) Representative traces of the heat of Ca^{2+} binding to the indicated tandem C2 domain constructs; $n \geq 4$. (D) Binding isotherms for WT C2AB (from Figure 1D), 3×C2AB, and YHRD mutant forms of each are shown for comparison; error bars represent SEM. Thermodynamic parameters are provided in Table 2.

3×-linker construct was previously described (Liu *et al.*, 2014). These mutations did not appear to disrupt the folding of any of these constructs, as evidenced by circular dichroism spectroscopy (Supplemental Figure S3).

ITC was performed on each of these constructs; Figure 2B shows a representative gel documenting that equal amounts of protein were analyzed. C2AB-YHRD, as compared with WT C2AB, exhibited a shift in endothermic peaks to higher molar ratios (Figure 2, C and D), indicating that a greater concentration of Ca^{2+} was required to reach saturation. The 3×C2AB gave rise to a small endothermic signal that became apparent only late in the titration, while 3×C2AB-YHRD yielded a larger endothermic signal that failed to fully saturate (Figure 2, C and D). From these traces, it is apparent that the YHRD mutations affected the ability of WT and 3×C2AB to bind Ca^{2+}. We note that the observed changes in enthalpy are not due to structural changes induced by Ca^{2+} binding (Supplemental Figure S3). Isotherms were fitted with a four-site sequential binding-site model; all thermodynamic parameters are provided in Table 2 (the signals from 3×C2AB were too small to fit). There was a significant decrease in the Ca^{2+} affinity of C2AB-YHRD compared with WT C2AB; a decrease in Ca^{2+} affinity was also apparent in 3×C2AB YHRD (Table 2). As a control, ITC was performed on isolated C2A and isolated C2B harboring the YH or RD substitutions, respectively (Supplemental Figure S4). The Ca^{2+}-binding energetics of the mutants were identical to their WT counterparts (Supplemental Table S3); hence the YHRD mutations affect Ca^{2+}-binding activity only in the context of the tandem C2 domains of syt-1. These findings further confirm the idea that C2A and C2B functionally interact with one another and help to provide a physical basis for how this interdomain communication occurs.

AFM was performed to determine whether the observed alterations in the intrinsic Ca^{2+}-binding properties of the YHRD mutants were due to the inability of C2A and C2B to physically interact with one another. We first attempted to compare the maximum lengths of WT C2AB and C2AB-YHRD. However, the potential change in length was not detected by this method, as the native linker is short (~2.6 nm), so the C2 domains are always in close proximity. However, in 3×C2AB, the linker is long enough to see increases in the maximal length of the protein by AFM, provided that C2A and C2B do not interact with one another (Figure 3; Liu *et al.*, 2014). As shown in Figure 3A, both 3×C2AB and 3×C2AB-YHRD formed both globular and dumbbell structures; each lobe of the dumbbell corresponds to a single C2 domain. However, dumbbells occurred more frequently for 3×C2AB-YHRD as compared with 3×C2AB (2.5-fold increase), suggesting that the YHRD mutations disrupt physical interactions between C2A and C2B. To quantitatively address this, we measured the maximum distances for each set of particles and observed a significant increase in the length of 3×C2AB-YHRD as compared with 3×C2AB (Figure 3B; $p < 0.001$). Apparently, the YHRD mutations disrupt interactions between C2A and C2B, allowing the domains to become more readily separated in space.

YHRD mutations impair syt-1 function in vitro

Syt-1 interacts with membranes (Perin *et al.*, 1990; Brose *et al.*, 1992) and t-SNAREs (Bennett *et al.*, 1992; Schiavo *et al.*, 1997;

	K_d (μM)	ΔH (cal/mol)	ΔS (cal/mol/K)	ΔG (kcal/mol)
C2AB	K_{d1} = 26.2 ± 7.6	ΔH_1 = 304 ± 110	ΔS_1 = 22.4 ± 0.41	ΔG_1 = –6.37 ± 0.13
	K_{d2} = 186 ± 26	ΔH_2 = 577 ± 99	ΔS_2 = 19.2 ± 0.32	ΔG_2 = –5.21 ± 0.12
	K_{d3} = 300 ± 64	ΔH_3 = 520 ± 410	ΔS_3 = 18.2 ± 1.2	ΔG_3 = –4.89 ± 0.12
	K_{d4} = 1750 ± 330	ΔH_4 = 2340 ± 820	ΔS_4 = 20.7 ± 2.6	ΔG_4 = –3.83 ± 0.11
C2AB-YHRD	K_{d1} = 173 ± 41	ΔH_1 = 576 ± 140	ΔS_1 = 19.3 ± 0.52	ΔG_1 = –5.17 ± 0.13
	K_{d2} = 499 ± 150	ΔH_2 = 1480 ± 510	ΔS_2 = 20.5 ± 1.7	ΔG_2 = –4.62 ± 0.23
	K_{d3} = 828 ± 160	ΔH_3 = 2410 ± 740	ΔS_3 = 22.2 ± 1.7	ΔG_3 = –4.23 ± 0.007
	K_{d4} = 2920 ± 690	ΔH_4 = –816 ± 630	ΔS_4 = 9.08 ± 2.2	ΔG_4 = –3.51 ± 0.14
3×C2AB-YHRD	K_{d1} = 274 ± 58	ΔH_1 = –239 ± 89	ΔS_1 = 15.3 ± 0.72	ΔG_1 = –4.78 ± 0.13
	K_{d2} = 533 ± 80	ΔH_2 = 1340 ± 340	ΔS_2 = 18.9 ± 1.1	ΔG_2 = –4.31 ± 0.12
	K_{d3} = 1099 ± 75	ΔH_3 = 1190 ± 340	ΔS_3 = 17.3 ± 1.2	ΔG_3 = –3.89 ± 0.042
	K_{d4} = 1680 ± 240	ΔH_4 = 461 ± 690	ΔS_4 = 15.0 ± 2.9	ΔG_4 = –4.01 ± 0.20

Representative traces and isotherms are shown in Figure 2. Data are presented as mean ± SEM, $n \geq 4$.

TABLE 2: Thermodynamic parameters of Ca^{2+} binding to C2AB domains of WT and YHRD mutant forms of syt-1.

Davis *et al.*, 1999), in a Ca^{2+}-promoted manner. We next determined whether the YHRD mutations altered these interactions. A cosedimentation assay was used to monitor the ability of syt-1 to bind to liposomes bearing phosphatidylserine (PS); depletion of the supernatant was monitored as a function of [Ca^{2+}]. In the presence of Ca^{2+}, all constructs were able to bind to membranes, but the YHRD mutant versions of C2AB and 3×C2AB were less sensitive to Ca^{2+} (Figure 4A); these were relatively small, but significant, reductions in the apparent affinity for Ca^{2+}.

Next coflotation assays were performed using PS-free proteoliposomes containing preformed t-SNARE (syntaxin-1A [syx] and SNAP-25B) heterodimers. The omission of PS allows direct binding of syt-1 to t-SNAREs to be measured, rather than syt•membrane interactions. All constructs exhibited some degree of binding in EGTA, but binding was significantly enhanced upon the addition of Ca^{2+} (Figure 4B). Under these conditions, no significant differences were observed between C2AB/C2AB-YHRD and 3×C2AB/3×C2AB-YHRD. Ca^{2+} titrations cannot be readily carried out in the assay system, so we varied the Ca^{2+} in the following experiments, using a version of the lipid-mixing assay in which syt-1 must bind to t-SNAREs in order to accelerate fusion.

To determine whether the YHRD mutations had an effect on the ability of syt-1 to stimulate fusion, we used a well-characterized in vitro lipid-mixing assay that mimics SV fusion with the plasma membrane in neurons (Tucker *et al.*, 2004; Bhalla *et al.*, 2006). In the "standard" assay, using preassembled t-SNARE heterodimers (Figure 4C), 3×C2AB-YHRD was less sensitive to Ca^{2+} as compared with 3×C2AB; no differences were observed between WT C2AB and C2AB-YHRD (Figure 4D). In the "split" t-SNARE version of the assay, only syx is reconstituted and soluble SNAP-25B is added in a soluble form; for fusion to occur Ca^{2+}•syt-1 must first bind and fold SNAP-25B onto syx (Figure 4E). In this experimental setup, the Ca^{2+} sensitivity of C2AB and C2AB-YHRD were again similar, and differences were uncovered using the 3×C2AB background, as 3×C2AB-YHRD clearly required higher [Ca^{2+}] than did 3×C2AB (Figure 4F). These in vitro assays are relatively insensitive to manipulations known to strongly affect SV exocytosis in neurons, so it is not surprising that the 3×C2AB background revealed differences resulting from additional mutations, as the 3×C2AB construct has partially impaired function (Liu *et al.*, 2014).

The syt-1 constructs were also analyzed in a content-mixing assay. Sulforhodamine B was encapsulated in v-SNARE liposomes and incubated with syx-only t-SNARE liposomes plus soluble SNAP-25B. As a result of sulforhodamine B self-quenching at high concentrations, content mixing is monitored as an increase in the fluorescence signal due to vesicle fusion (Supplemental Figure S5A). Analogous

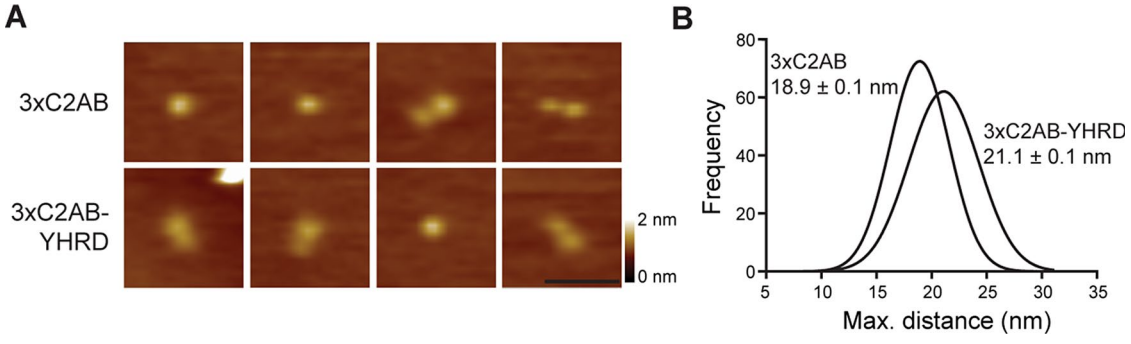

FIGURE 3: YHRD mutations increase the distance between the C2 domains of syt-1. (A) AFM images of 3×C2AB and 3×C2AB-YHRD; dumbbell-like structures (doublets) were more common in the 3×C2AB-YHRD than 3×C2AB. (B) Gaussian fits of frequency distributions of maximum linear dimensions of 3×C2AB and 3×C2AB-YHRD. The 3× mutant was used to uncover length differences resulting from substitution of YHRD, as changes in the length of WT C2AB background could not be detected by AFM (unpublished data). The peaks of the distributions ± SEM are indicated; $p < 0.001$. $n = 248$ for both samples. Scale bar: 50 nm; color-height scale: 0–2 nm.

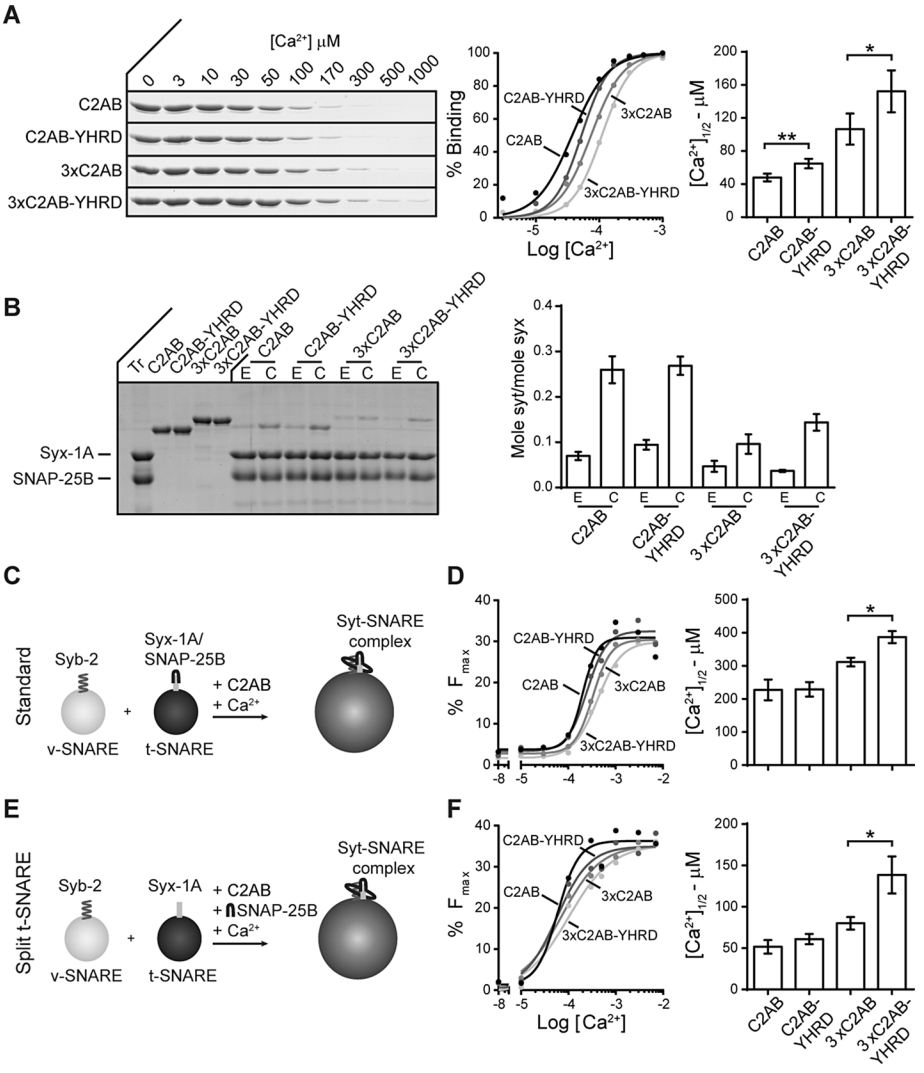

FIGURE 4: YHRD mutations increase the Ca^{2+} requirements for effector binding and membrane fusion in vitro. (A) Binding of syt-1 to PS-bearing liposomes was monitored via a cosedimentation assay. Representative SDS–PAGE gels showing protein depletion of the supernatant in the presence of increasing free [Ca^{2+}] are shown (left). The percentage of bound protein was calculated (middle) and used to determine the $[Ca^{2+}]_{1/2}$ (right); $n = 4$. (B) A coflotation assay was used to measure binding of syt-1 to t-SNAREs in the presence (1 mM free Ca^{2+}; C) and absence (0.2 mM EGTA; E) of Ca^{2+}; a representative SDS–PAGE gel is shown (left). Bound protein was quantified and normalized to syx (right); $n = 3$. (C) Schematic illustration of the standard in vitro lipid-mixing assay in which preassembled t-SNARE heterodimer vesicles are incubated with v-SNARE vesicles. (D) The extent of fusion (80 min) was plotted as a function of free [Ca^{2+}] (left) and used to calculate the $[Ca^{2+}]_{1/2}$ values (right); $n = 4$. (E) "Split" t-SNARE lipid-mixing assay in which syx was reconstituted and SNAP-25B was added in a soluble form; Ca^{2+}•syt-1 must fold SNAP-25B onto syx to facilitate lipid mixing. (F) As in D, data were plotted (left) and used to determine the $[Ca^{2+}]_{1/2}$ values (right); $n \geq 3$. Error bars indicate SEM; *, $p < 0.05$; **, $p < 0.01$.

to the results obtained using the lipid-mixing assay, 3×C2AB-YHRD was not as efficient at driving content mixing as 3×C2AB, and differences between C2AB and C2AB-YHRD could not be detected (Supplemental Figure S5, B and C).

The YHRD mutations reduce evoked but not spontaneous neurotransmission

In the final series of experiments, we determined whether the YHRD mutations affected SV exocytosis in cultured neurons. Hippocampal neurons from WT or syt-1 knockout (KO) mice expressing full-length versions of WT, YHRD, 3×, and 3×-YHRD mutant forms of syt-1 were analyzed. Coimmunostaining with an SV marker, synaptophysin, confirmed that each construct was expressed and correctly targeted to synapses (Supplemental Figure S6, A and B).

A secondary function of syt-1 is to serve as a fusion clamp that arrests SNARE-catalyzed fusion before the arrival of the Ca^{2+} trigger (Chicka *et al.*, 2008; Liu *et al.*, 2014). We first determined whether the YHRD mutations altered clamping activity by monitoring miniature excitatory postsynaptic currents (mEPSC) in WT or KO neurons expressing each of the constructs listed above (Figure 5A). The mEPSC amplitudes were the same in all conditions (Figure 5B). Moreover, all of the mutant constructs were able to clamp the elevated mEPSC frequency characteristic of syt-1 KO neurons (Figure 5C). Thus the YHRD mutations do not appear to affect the function of syt-1 during spontaneous release.

Next we carried out whole-cell voltage-clamp experiments to measure evoked excitatory postsynaptic currents (EPSCs) regulated by each of the mutant forms of syt-1. The amplitude and total charge of KO neurons expressing YHRD were significantly reduced as compared with neurons expressing the WT protein (Figure 6, A–C). The same trend was also observed in neurons expressing 3× and 3×-YHRD (Figure 6, A–C). Analysis of the total charge transfer, fitted with a double exponential function, revealed that neurons expressing the YHRD and 3× mutant form of syt-1 had kinetics that were virtually identical to WT (Figure 6D). Strikingly, we observed that 3×-YHRD was virtually devoid of function during evoked transmission (Figure 6, A–D), while the 3× mutant supported a limited amount of SV release (Figure 6, A–D; Liu *et al.*, 2014). The addition of the YHRD mutations abolished the residual function of this construct, potentially because the latter mutations disrupt the ability of C2A and C2B to interact. EPSCs of syt-1 KO neurons expressing WT or YHRD were also analyzed at increasing extracellular [Ca^{2+}]. Again, a significant decrease in amplitude was observed for neurons expressing YHRD as compared with those expressing WT (Figure 6E).

It should be noted that the inefficient rescue by the YHRD mutants could result from reductions in the size of the readily releasable pool (RRP) of SVs (Rosenmund and Stevens, 1996). To address this, we measured the RRP by applying hypertonic sucrose. All of the constructs were able to completely rescue the size of the RRP caused by loss of syt-1 (Supplemental Figure S6, C and D). Hence the loss of function reported here is due to reductions in the ability of syt-1 to drive exocytosis and is not secondary to upstream effects on vesicle availability or priming.

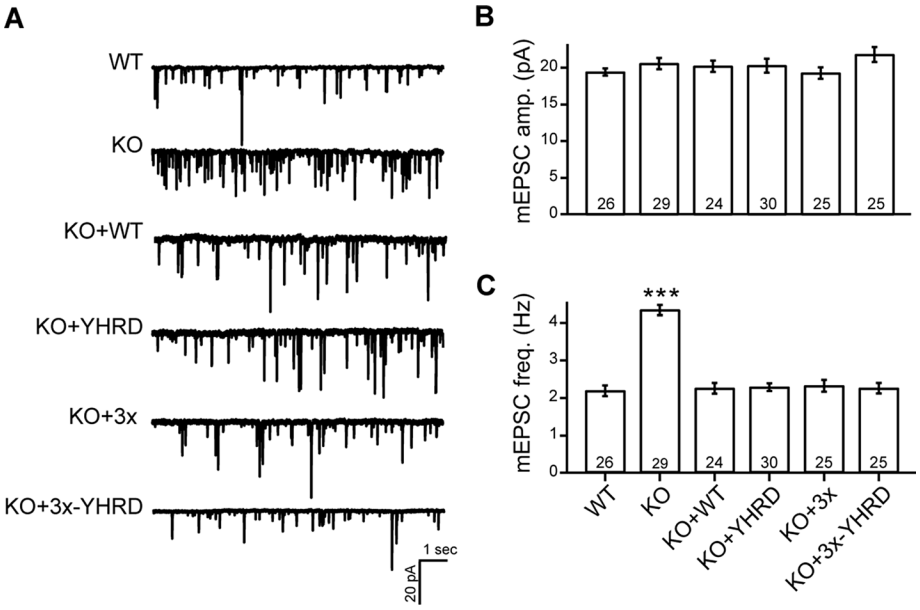

FIGURE 5: Spontaneous release is unaffected by the YHRD mutations. (A) Representative mEPSC traces recorded from WT, syt-1 KO, and KO neurons expressing WT, YHRD, 3×, and 3×-YHRD mutant forms of syt-1. (B and C) Bar graphs showing mEPSC amplitude (pA; B) and frequency (Hz; C). The number of neurons in each group are indicated; plotted values represent the mean ± SEM. ***, $p < 0.001$.

DISCUSSION

X-ray crystallographic studies of the cytoplasmic domains of syt-1 and syt-3 revealed different apparent states of these proteins (Sutton *et al.*, 1999; Fuson *et al.*, 2007; Vrljic *et al.*, 2010); the main differences concerned the relative configuration of the tandem C2 domains. In one structure, C2A and C2B were in an "open" state, in which only the metal/phospholipid-binding loops were adjacent to one another, with no indication of inter–C2-domain interactions (Sutton *et al.*, 1999). In contrast, in another C2AB structure, C2A and C2B were in a "closed" conformation, in which a clear physical association between the tandem C2 domains was apparent (Fuson *et al.*, 2007). The major differences observed between the "open" and "closed" states of C2AB were the lack of coupling between Y180 and H237, and the formation of tight salt bridges between C2A residues D178 in loop 1, R199 in loop 2, R233 in loop 3 and two exposed residues (R388 and D392) on the outward facing hydrophilic side of the α-helical insertion in C2B.

NMR has been used to gain a more dynamic view of the structure of syt-1 in solution, but this approach is limited by the relatively large size of the cytoplasmic domain. In one study, it was concluded that C2A and C2B do not interact (Araç *et al.*, 2006), whereas another NMR study supported the idea that the tandem C2 domains likely conform to a small number of favored states (Seven *et al.*, 2013), implying the occurrence of interdomain contacts. Thermodynamic and modeling studies also indicated that syt-1 occupies an ensemble of conformational states (Gauer *et al.*, 2012; Bykhovskaia, 2015). Additionally, it was proposed that interdomain interactions between the Ca^{2+}-binding loops in C2A and the helical insertion in C2B stabilized the structure (Bykhovskaia, 2015). So, the structure by Fuson *et al.* (2007) most likely corresponds to one of these favored states.

Here we show that substitution of the YHRD residues (with a Phe and three Ala), in a 3×-linker background, increased the length of the cytoplasmic domain of syt-1. It should be noted that increasing the linker region alone (i.e., 3×C2AB) did not change the overall length of the protein (Figure 3; Liu *et al.*, 2014), presumably because C2A and C2B physically interact. Therefore the observed changes in length are due to loss of interfacial interactions. This effect was associated with a reduction in the intrinsic affinity of syt-1 for Ca^{2+} (Figure 2), a rightward shift in the Ca^{2+} requirements for binding to membranes, and in the ability of syt-1 to drive lipid mixing in vitro (Figure 4). Finally, the YHRD mutant had a diminished ability to drive exocytosis when expressed in syt-1 KO neurons (Figure 6). Moreover, the 3×-YHRD mutant completely failed to trigger SV exocytosis (Figure 6). We conclude that these residues—YHRD—participate in the intramolecular interactions within syt-1 and that these interactions contribute to function.

The findings reported here are consistent with a recent study that made use of long polyproline rods that precluded interactions between C2A and C2B, resulting in a loss of function (Liu *et al.*, 2014). Here we made similar observations by mutating residues to disrupt contact between these C2 domains. These results may potentially help to explain a number of conundrums concerning the biochemical and functional properties of syt-1. For example, mutations that disrupt Ca^{2+} binding to C2A have little effect on the function of syt (Fernandez-Chacon *et al.*, 2002; Robinson *et al.*, 2002; Stevens and Sullivan, 2003), but a mutation in C2A (R233Q) that shifted only the Ca^{2+} dose response for lipid binding, resulted in a marked loss of function during synaptic transmission (Fernandez-Chacon *et al.*, 2001) and reduced catecholamine release from PC12 cells (Wang *et al.*, 2003). We speculate that the former mutations do not affect the synergy between the tandem C2 domains (Supplemental Figure S2; Radhakrishnan *et al.*, 2009), but perhaps the latter mutation has a profound effect on communication between the domains, because R233 is known to form a salt bridge with D392 of C2B (Fuson *et al.*, 2007). In this view, mutations in C2A affect the function of syt-1 by interfering with the function of the adjacent domain. In the case of syt-1, the C2B domain is the crucial Ca^{2+}-sensing element (Mackler *et al.*, 2002; Nishiki and Augustine, 2004), so R233 is likely to inhibit the function of the latter C2 domain. In addition, a previous study reported that isolated C2B has relatively poor membrane penetration activity, unless tethered to C2A (Bai *et al.*, 2002). Surprisingly, even a "dead" C2A domain (D230,232N), which does not bind Ca^{2+}, was able to facilitate the membrane-penetration activity of the C2B domain. Again, the physical interaction with C2A might serve to confer functionality to the C2B domain; indeed, interfacial contacts were not altered by these two specific mutations.

Roughly a third of proteins that harbor a C2 domain contain more than one, depending on the species, suggesting frequent duplications of this motif. After duplication, the findings reported here suggest that the C2 domains subsequently evolved to interact and function in tandem. Alternatively, another interpretation is conceivable: C2 domains might have first evolved the ability to interact with one another via intermolecular interactions. Then, upon duplication within a parent protein, these motifs engaged in intramolecular interactions (Tucker and Chapman, 2002). In any case, the presence of more than one C2 domain endows proteins with the potential ability

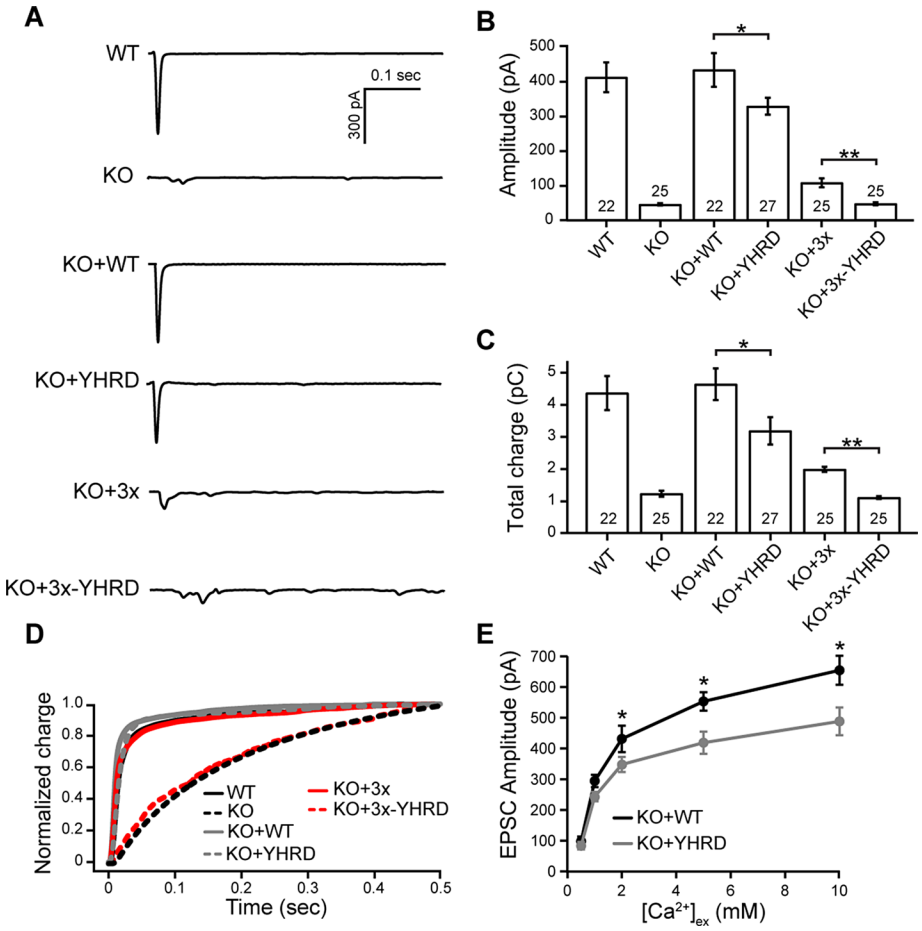

FIGURE 6: The YHRD mutations decrease evoked neurotransmission in cultured hippocampal neurons. (A) Representative evoked EPSC traces recorded from WT, syt-1 KO, and KO neurons expressing WT, YHRD, 3×, and 3×-YHRD constructs. (B and C) Bar graphs of evoked EPSC amplitude (pA; B) and total charge (pC; C). The number of neurons in each group are indicated inside the bars. (D) Normalized cumulative total charge transfer, averaged for each group; a double exponential function was used to fit the data. (E) Representative evoked EPSCs recorded from KO neurons expressing WT or YHRD in the presence of the indicated extracellular Ca^{2+} concentration, $[Ca^{2+}]_{ex}$. There were 10–20 neurons analyzed per condition. All data represent mean ± SEM; *, $p < 0.05$; **, $p < 0.01$.

to conform to an ensemble of states, determined by the relative orientation of two or more C2 domains, allowing them to bind and interact with effectors in ways not possible with a single C2 domain. This results in a richer, more complex repertoire of biochemical properties. In the case of syt-1, the tandem C2 domains synergistically interact with each other to facilitate membrane fusion. Indeed, the residues YHRD are conserved among a number of syt isoforms and likely mediate interactions between their C2 domains.

While the current study focuses on the C2 domains of syt-1, it still remains to be determined whether the C2 domains in other proteins engage in intramolecular interactions or whether such putative interactions contribute to function. For example, the ferlin family contains five to seven C2 domains, the most of any protein family (Lek *et al.*, 2012). Otoferlin, a ferlin expressed in cochlear hair cells, has six C2 domains; five of the six can stimulate membrane fusion, in vitro, in a Ca^{2+}-dependent manner (Johnson and Chapman, 2010). It is plausible that otoferlin and other large multi C2-domain proteins engage in complex intramolecular interactions that contribute to function. Future studies are needed to examine the synergy between these domains and to establish the generality of the findings reported here.

MATERIALS AND METHODS

Phospholipids

1-Palmitoyl-2-oleoyl-*sn*-glycero-3-phosphoethanolamine (phosphatidylethanolamine, PE), 1,2-dioleoyl-*sn*-glycero-3-phospho-L-serine (PS), 1-palmitoyl-2-oleoyl-*sn*-glycero-3-phosphocholine (phosphatidylcholine, PC), 1,2-dipalmitoyl-*sn*-glycero-3-phosphoethanolamine-*N*-(7-nitro-2-1,3-benzoxadiazol-4-yl) (NBD-PE), and *N*-(lissamine rhodamine B sulfonyl)-1,2-dipalmitoyl-*sn*-glycero-3-phosphoethanolamine (Rho-PE) were purchased from Avanti Polar Lipids (Alabaster, AL).

Recombinant proteins and protein purification

Rat syt-1 cDNA encoding the cytoplasmic domain (denoted C2AB, residues 96–421; Perin *et al.*, 1990) was provided by T. C. Südhof (Stanford University, Stanford, CA); the D374 mutation was repaired by substitution with a glycine residue. The 3×C2AB linker mutant form of WT syt-1 C2AB was previously described (Liu *et al.*, 2014).

YHRD point mutants (Y180F, H237A, R388A, and D392A), and Ca^{2+} ligand point mutants (D178,230,232 and D309,363,365; substituted to Ala or Asn), were generated using a QuikChange Site-Directed Mutagenesis Kit (Agilent Technologies, Santa Clara, CA). C2AB and mutant forms of syt-1, isolated C2A (residues 96–265), and isolated C2B (residues 248–421) were subcloned into pGEX-4T vectors and expressed as glutathione *S*-transferase (GST)-tagged fusion proteins, purified utilizing glutathione–Sepharose beads (GE Healthcare, Little Chalfont, United Kingdom), and cleaved with thrombin to remove the GST-tag, as previously described (Gaffaney *et al.*, 2008). cDNA encoding synaptobrevin-2 (syb) and syx was provided by J. E. Rothman (Yale University, New Haven, CT), and SNAP-25B was provided by M. C. Wilson (University of New Mexico Health Sciences Center, Albuquerque, NM). All three full-length SNARE proteins were individually subcloned into a pTrcHis vector, and the cytoplasmic domain of syb (cd-Syb; residues 1–94) was subcloned into a pET vector. SNAP-25B and syx were also subcloned into a pRSFDuet vector. All of these SNARE proteins were expressed as His_6-tagged fusion proteins and purified using Ni-Sepharose beads (GE Healthcare), as previously described (Gaffaney *et al.*, 2008).

Circular dichroism

WT and mutant forms of syt-1 C2AB were buffer exchanged into 40 mM Tris (pH 7.4) and 100 mM NaCl. For each sample, the protein concentration was 0.2 mg/ml, and spectra were obtained in 0.2 mM EGTA or 1 mM Ca^{2+} (free), using a 1 mm path–length cuvette, at room temperature (RT). Baseline corrections were made by subtracting the buffer spectrum. Data were obtained and analyzed

using a Model 420 circular dichroism spectrophotometer and software package (Aviv Biomedical, Lakewood, NY).

ITC

WT and mutant forms of syt-1 were dialyzed overnight against 50 mM HEPES-NaOH (pH 7.4), 200 mM NaCl, and 10% glycerol; the buffer was previously treated with Chelex-100 resin (Bio-Rad, Hercules, CA) to remove divalent cations. After this, the dialysis buffer was filtered and used to make all protein and Ca^{2+} dilutions. Samples were degassed before each experiment. Heat of binding was measured by 20 consecutive injections of Ca^{2+} into a sample cell containing the protein of interest. Protein concentrations were 75 µM and 200–500 µM for the specified "low-" and "high-" concentration experiments, respectively. Corrections for heat of dilution were done by subtracting the signal of Ca^{2+} into buffer. Experiments were performed using a MicroCal iTC_{200} (Malvern Instruments, Malvern, United Kingdom), and data were analyzed using a Sequential Binding Site model in the software package.

AFM

The 3×C2AB and 3×C2AB-YHRD were diluted in HEPES-buffered saline (HBS) to 0.4 nM, and 45 µl of each sample was deposited onto freshly cleaved mica (10-mm-diameter disks). After a 5-min adsorption period, the samples were rinsed with Biotechnology Performance Certified water (Sigma-Aldrich, St. Louis, MO) to remove unabsorbed protein and dried under a stream of nitrogen gas. AFM imaging was carried out using a Multimode AFM equipped with a J-scanner and a Nanoscope IIIa controller (Bruker Digital Instruments, Billerica, MA). All samples were imaged in tapping mode in air, using silicon nitride probes (OTESPA; Bruker AFM Probes). These cantilevers had a spring constant of ~40 N/m and a drive frequency of ~300 kHz (10–20% below the resonance frequency). The applied imaging force was kept as low as possible ($A_S/A_0 \sim 0.85$). Images were captured at a scan rate of 4 Hz, with 512 scan lines per area. Data analysis was performed using Nanoscope version 5.31r1 software (Bruker Digital Instruments). Protein length was determined by drawing a cross-section along the imaged protein structures.

Liposome and vesicle preparation

Protein-free liposomes were prepared by mixing lipids (15% PS, 30% PE, 55% PC) in chloroform and drying the mixture under nitrogen. The dried film was resuspended in 50 mM HEPES-NaOH (pH 7.4), 100 mM NaCl. Liposomes were generated by extrusion through a 100-nm polycarbonate membrane (Whatman, GE Healthcare, Little Chalfont, United Kingdom).

For SNARE-bearing vesicles used in reconstituted in vitro lipid-mixing assays, the lipid compositions were 15% PS, 27% PE, 55% PC, 1.5% NBD-PE, and 1.5% Rho-PE for v-SNARE vesicles and 15% PS, 30% PE, and 55% PC for t-SNARE heterodimer or syx-only vesicles. For coflotation assays, the lipid composition was 30% PE and 70% PC. SNARE-bearing vesicles were prepared as previously described (Tucker *et al.*, 2004).

Cosedimentation assays

WT or mutant forms of syt-1 C2AB (4 µM) were mixed with PS-bearing liposomes (15% PS, 30% PE, 55% PC) in HEPES buffer (25 mM HEPES-NaOH, pH 7.4, 100 mM KCl), in the presence of the indicated free [Ca^{2+}] and centrifuged at 170,000 × *g* at 4°C for 45 min in a Optima MAX-E tabletop ultracentrifuge (Beckman Coulter, Brea, CA). The supernatant from each sample was collected, and depletion was analyzed by SDS–PAGE and Coomassie blue staining. Bands were quantified by densitometry to determine the amount of unbound protein; these data were used to calculate the percentage of bound protein, which was then plotted versus the free [Ca^{2+}]; $[Ca^{2+}]_{1/2}$ values were determined by fitting the data using Prism 6 software (GraphPad, La Jolla, CA). A paired two-tailed Student's *t* test was used to determine whether the $[Ca^{2+}]_{1/2}$ values were significantly different.

Coflotation assays

The ability of syt-1 to bind to t-SNAREs was determined using a coflotation assay, as previously described (Tucker *et al.*, 2004). WT or mutant forms of syt-1 C2AB (10 µM) were incubated with 45 µl t-SNARE–bearing vesicles (PS-free) in the presence or absence of 1 mM Ca^{2+}. After 60 min, samples were loaded onto the bottom of a four-step Accudenz (Accurate Chemical & Scientific Corporation, Westbury, NY) gradient and centrifuged at 287,000 × *g* at 4°C for 2 h. Samples were collected and subjected to SDS–PAGE and Coomassie blue staining. Bands were quantified using densitometry and normalized to the syx band in each lane; 0.6 µg protein was loaded in control lanes.

In vitro lipid-mixing assays

Lipid-mixing assays were carried out as described previously (Tucker *et al.*, 2004; Bhalla *et al.*, 2006). Briefly, lipid mixing between v-SNARE vesicles (Vr; "r" refers to reconstituted) and t-SNARE heterodimer vesicles (Tr) or syx-only vesicles (Syxr) was monitored via dequenching of the NBD donor using a Synergy HT multidetection microplate reader (Bio-Tek, Winooski, VT). In reactions, 1 µM of WT or mutant forms of syt-1 C2AB, 0.2 mM EGTA, Vr, and Tr (for standard assays) or Syxr plus 5 µM soluble SNAP-25B (for split t-SNARE assays) were incubated at 37°C for 20 min. The indicated free [Ca^{2+}] was then added, and the reaction was monitored for an additional 60 min. At the conclusion of the experiment, 2.5% *n*-dodecyl-β-D-maltoside was added to yield the maximum fluorescence signal, which was then used for normalization. The extent of fusion at t = 80 min was plotted as a function of free [Ca^{2+}]. Prism 6 software (GraphPad) was used to determine the $[Ca^{2+}]_{1/2}$ values. An unpaired Student's *t* test was used to determine the significance of the $[Ca^{2+}]_{1/2}$ differences resulting from the YHRD mutations.

In vitro content-mixing assay

Proteoliposomes for the content-mixing assay, using sulforhodamine B, were prepared as reported previously, with modifications (Lai *et al.*, 2015; Lou *et al.*, 2015). The lipid composition for both Vr and Syxr were 15% PS, 30% PE, and 55% PC. Dried lipid films were suspended in dialysis buffer (25 mM HEPES-NaOH, pH 7.4, 100 mM KCl); to make Vr, the buffer also contained 20 mM sulforhodamine B. After five freeze–thaw cycles, protein-free large unilamellar vesicles (~100 nm in diameter) were prepared by extrusion through a 100-nm polycarbonate filter (Whatman). For Syxr, syx was mixed with protein-free liposomes in dialysis buffer plus 0.8% octylglucoside at 4°C for 15 min. The liposome/protein mixture was diluted twofold with dialysis buffer and dialyzed overnight at 4°C. Preparation of Vr was the same as above, except that 20 mM sulforhodamine B was present in the dialysis buffer for dilution; after dialysis, free sulforhodamine B was removed using the PD-10 desalting column (GE Healthcare).

The content-mixing assay was carried out in the same manner as the lipid-mixing assay, except the sulforhodmine B fluorescence signal was monitored. Briefly, 2 µM of WT or mutant forms of syt-1 C2AB, 5 µM SNAP-25B, Syxr and Vr (at a 9:1 ratio), and 0.2 mM EGTA were mixed and incubated at 37°C for 20 min. Ca^{2+} (500 µM

free concentration) was added, and the reaction was monitored for an additional 60 min. For control experiments, 10 μM of the cd-Syb was used. An increase in fluorescence intensity, due to fluorescence dequenching of sulforhodamine B, reports content mixing. The highest fluorescence intensity was obtained by adding 2.5% *n*-dodecyl-β-D-maltoside, which was used for normalization. An unpaired Student's *t* test was used to determine the significance of the differences in fusion activity resulting from the YHRD mutations.

Cell culture and viral infection

Hippocampal cultures were prepared from syt-1 KO mice (Jackson Laboratory, Bar Harbor, ME) in accordance with the guidelines of the National Institutes of Health (NIH), as approved by the Animal Care and Use Committee at the University of Wisconsin–Madison (protocol number M01221-0-06-14). Hippocampal neurons were dissected from newborn mice and incubated in a digestion solution that contained 0.25% trypsin-EDTA (Corning, Corning, NY), 20 mM glucose, and 25 U/ml DNase. The tissue was washed using Hank's buffered salt solution plus 5 mM HEPES (Corning), 20 mM D-glucose, and 10% fetal bovine serum (Gibco, Thermo Fisher Scientific, Waltham, MA), mechanically dissociated in culture medium, and plated on poly-D-lysine (Life Technologies, Thermo Fisher Scientific, Waltham, MA)–coated glass coverslips. Cells were grown in Neurobasal-A culture medium (Gibco) supplemented with 2% B27 (Gibco) and 2 mM Glutamax (Invitrogen, Thermo Fisher Scientific, Waltham, MA). Cultures were maintained at 37°C in a 5% CO_2-humidified incubator.

For electrophysiological recordings, cDNA encoding full-length versions of WT and 3× and YHRD mutant forms were subcloned into a modified pLOX vector (Addgene, Cambridge, MA). Lentiviral particles were generated by cotransfecting pLOX vectors with two other packaging vectors (vesicular stomatitis virus G glycoprotein and Delta 8.9) into HEK293T cells. The supernatant was collected after 48–72 h, purified by filtration through a 0.45-μm filter, and centrifuged at 25,000 rpm for 2 h to concentrate virus. Viral particles were resuspended in phosphate-buffered saline (PBS) and used to infect syt-1 KO neurons at 5 DIV (days in vitro).

Immunocytochemistry

At 14–15 DIV, hippocampal neurons were fixed for 10 min with 4% paraformaldehyde (wt/vol) in PBS, permeabilized for 10 min in 0.1% Triton X-100 (vol/vol), and blocked for 60 min with 10% bovine serum albumin (wt/vol) plus 0.1% Triton X-100 (vol/vol). Coverslips were then incubated with primary antibodies at RT for 2 h. A monoclonal mouse antibody that recognizes the luminal domain of syt-1 (41.1; SYnaptic SYstems, Göttingen, Germany; 1:1000 dilution), was used to determine syt-1 localization. Nerve terminals were identified using a polyclonal guinea pig anti-synaptophysin antibody (SYnaptic SYstems; 1:1000 dilution). Samples were washed with PBS three times, and then stained with Alexa Fluor 488–tagged anti-mouse (1:1000 dilution), and Alexa Fluor 594–tagged anti-guinea pig (1:1000 dilution) secondary antibodies (Jackson ImmunoResearch Laboratories, West Grove, PA) for 1 h. Coverslips were washed three times with PBS and mounted in Fluoromount mounting medium (Southern Biotechnology Associates, Birmingham, AL). Images were collected from a FV1000 upright laser-scanning confocal microscope with FV10-ASW 3.1 acquisition software (Olympus, Center Valley, PA), using a 60×/1.40 NA oil objective at RT, under identical laser and gain settings. To quantify the colocalization of syt-1 or mutants with synaptophysin, we calculated the Mander's coefficient of each image using ImageJ software (NIH, Bethesda, MD) with the JACoP plug-in.

Electrophysiology

Whole-cell patch-clamp recordings of mEPSCs, evoked EPSCs, and hypertonic sucrose responses from neurons at 14–15 DIV, were performed in voltage-clamp mode using an EPC-10/2 amplifier (HEKA, Holliston, MA). The recording pipettes were pulled from borosilicate glass capillary tubes (Warner Instruments, Hamden, CT) and had resistances of 3–5 MΩ. Only whole-cell patches with series resistances <15 MΩ were used for recording, and the membrane potential was held at −70 mV. The pipette solution consisted of 130 mM K-gluconate, 1 mM EGTA, 5 mM Na-phosphocreatine, 2 mM Mg-ATP, 0.3 mM Na-GTP, 5 mM QX-314, and 10 mM HEPES (pH 7.3). The bath solution consisted of 128 mM NaCl, 30 mM glucose, 5 mM KCl, 5 mM $CaCl_2$, 1 mM $MgCl_2$, 50 mM D-AP5, 20 mM bicuculline, and 25 mM HEPES (pH 7.3). D-AP5, bicuculline, and QX-314 were obtained from TOCRIS Bioscience (Bristol, United Kingdom).

For mEPSC recordings, 1 μM tetrodotoxin (TOCRIS Bioscience) was added to the bath solution. For evoked EPSC recordings, presynaptic inputs were stimulated with a bipolar electrode (FHC, CBAEC75-Concentric Bipolar Electrode) that was placed 100–120 μm from the recording neuron. For hypertonic sucrose experiments, sucrose (500 mM) was puffed over the entire area that included all the presynaptic boutons contacting the recording neuron, using an air pressure system (PicoSpritzer III; Parker Hannifin, Cleveland, OH). All of the recordings were performed at RT and 2 mM, or the indicated Ca^{2+} concentration, in the bath solution.

All recordings were made from two to three coverslips, from two to three independent litters of animals. The numbers of cells are indicated in the figures or figure legends. Data were acquired using PATCHMASTER software (HEKA) and analyzed using MiniAnalysis software (Synaptosoft, Fort Lee, NJ), Clampfit (Molecular Devices, Sunnyvale, CA), and Igor (Wavemetrics, Portland, OR). Statistical significance was evaluated using the Kruskal-Wallis test for multiple comparisons of groups with nonnormal distributions. For groups with a normal distribution, statistical significance was determined using either the Student's test or by one-way analysis of variance.

ACKNOWLEDGMENTS

The authors thank the Chapman laboratory for discussion and comments on manuscript. This study was supported by a grant from the NIH (MH061876). C.S.E. was supported by a PhRMA Foundation predoctoral fellowship and by a UW–Madison Molecular and Cellular Pharmacology Training Grant (5T32-GM008688). R.B.S. was supported by an NIH grant (AR063634). P.J. and J.M.E. were funded by Kidney Research UK, and J.M.E. was funded by the Biotechnology and Biological Sciences Research Council (Grant BB/J018236/1). E.R.C. is an investigator of the Howard Hughes Medical Institute.

REFERENCES

Araç D, Chen X, Khant HA, Ubach J, Ludtke SJ, Kikkawa M, Johnson AE, Chiu W, Südhof TC, Rizo J (2006). Close membrane-membrane proximity induced by Ca^{2+}-dependent multivalent binding of synaptotagmin-1 to phospholipids. Nat Struct Mol Biol 13, 209–217.

Bai J, Wang P, Chapman ER (2002). C2A activates a cryptic Ca^{2+}-triggered membrane penetration activity within the C2B domain of synaptotagmin I. Proc Natl Acad Sci USA 99, 1665–1670.

Bennett MK, Calakos N, Scheller RH (1992). Syntaxin: a synaptic protein implicated in docking of synaptic vesicles at presynaptic active zones. Science 257, 255–259.

Bhalla A, Chicka MC, Tucker WC, Chapman ER (2006). Ca^{2+}-synaptotagmin directly regulates t-SNARE function during reconstituted membrane fusion. Nat Struct Mol Biol 13, 323–330.

Brose N, Petrenko AG, Südhof TC, Jahn R (1992). Synaptotagmin: a calcium sensor on the synaptic vesicle surface. Science 256, 1021–1025.

Bykhovskaia M (2015). Calcium binding promotes conformational flexibility of the neuronal Ca^{2+} sensor synaptotagmin. Biophys J 108, 2507–2520.

Chapman ER (2008). How does synaptotagmin trigger neurotransmitter release? Annu Rev Biochem 77, 615–641.
Chapman ER, Davis AF (1998). Direct interaction of a Ca^{2+}-binding loop of synaptotagmin with lipid bilayers. J Biol Chem 273, 13995–14001.
Chicka MC, Hui E, Liu H, Chapman ER (2008). Synaptotagmin arrests the SNARE complex before triggering fast, efficient membrane fusion in response to Ca^{2+}. Nat Struct Mol Biol 15, 827–835.
Damer CK, Creutz CE (1996). Calcium-dependent self-association of synaptotagmin I. J Neurochem 67, 1661–1668.
Davis AF, Bai J, Fasshauer D, Wolowick MJ, Lewis JL, Chapman ER (1999). Kinetics of synaptotagmin responses to Ca^{2+} and assembly with the core SNARE complex onto membranes. Neuron 24, 363–376.
Fealey ME, Gauer JW, Kempka SC, Miller K, Nayak K, Sutton RB, Hinderliter A (2012). Negative coupling as a mechanism for signal propagation between C2 domains of synaptotagmin I. PLoS One 7, e46748.
Fernandez I, Araç D, Ubach J, Gerber SH, Shin O, Gao Y, Anderson RG, Südhof TC, Rizo J (2001). Three-dimensional structure of the synaptotagmin 1 C2B-domain: synaptotagmin 1 as a phospholipid binding machine. Neuron 32, 1057–1069.
Fernandez-Chacon R, Konigstorfer A, Gerber SH, Garcia J, Matos MF, Stevens CF, Brose N, Rizo J, Rosenmund C, Südhof TC (2001). Synaptotagmin I functions as a calcium regulator of release probability. Nature 410, 41–49.
Fernandez-Chacon R, Shin OH, Konigstorfer A, Matos MF, Meyer AC, Garcia J, Gerber SH, Rizo J, Südhof TC, Rosenmund C (2002). Structure/function analysis of Ca^{2+} binding to the C2A domain of synaptotagmin 1. J Neurosci 22, 8438–8446.
Fuson KL, Montes M, Robert JJ, Sutton RB (2007). Structure of human synaptotagmin 1 C2AB in the absence of Ca^{2+} reveals a novel domain association. Biochemistry 46, 13041–13048.
Gaffaney JD, Dunning FM, Wang Z, Hui E, Chapman ER (2008). Synaptotagmin C2B domain regulates Ca^{2+}-triggered fusion in vitro: critical residues revealed by scanning alanine mutagenesis. J Biol Chem 283, 31763–31775.
Gauer JW, Sisk R, Murphy JR, Jacobson H, Sutton RB, Gillispie GD, Hinderliter A (2012). Mechanism for calcium ion sensing by the C2A domain of synaptotagmin I. Biophys J 103, 238–246.
Hui E, Gaffaney JD, Wang Z, Johnson CP, Evans CS, Chapman ER (2011). Mechanism and function of synaptotagmin-mediated membrane apposition. Nat Struct Mol Biol 18, 813–821.
Hui E, Johnson CP, Yao J, Dunning FM, Chapman ER (2009). Synaptotagmin-mediated bending of the target membrane is a critical step in Ca^{2+}-regulated fusion. Cell 138, 709–721.
Johnson CP, Chapman ER (2010). Otoferlin is a calcium sensor that directly regulates SNARE-mediated membrane fusion. J Cell Biol 191, 187–197.
Lai Y, Lou X, Diao J, Shin YK (2015). Molecular origins of synaptotagmin 1 activities on vesicle docking and fusion pore opening. Sci Rep 5, 9267.
Lek A, Evesson FJ, Sutton RB, North KN, Cooper ST (2012). Ferlins: regulators of vesicle fusion for auditory neurotransmission, receptor trafficking and membrane repair. Traffic 13, 185–194.
Liu H, Bai H, Xue R, Takahashi H, Edwardson JM, Chapman ER (2014). Linker mutations reveal the complexity of synaptotagmin 1 action during synaptic transmission. Nat Neurosci 17, 670–677.
Lou X, Shin J, Yang Y, Kim J, Shin YK (2015). Synaptotagmin-1 is an antagonist for Munc18–1 in SNARE zippering. J Biol Chem 290, 10535–10543.
Mackler JM, Drummond JA, Loewen CA, Robinson IM, Reist NE (2002). The C(2)B Ca^{2+}-binding motif of synaptotagmin is required for synaptic transmission in vivo. Nature 418, 340–344.
Martens S, Kozlov MM, McMahon HT (2007). How synaptotagmin promotes membrane fusion. Science 316, 1205–1208.
Matthew WD, Tsavaler L, Reichardt LF (1981). Identification of a synaptic vesicle-specific membrane protein with a wide distribution in neuronal and neurosecretory tissue. J Cell Biol 91, 257–269.
Nalefski EA, Falke JJ (1996). The C2 domain calcium-binding motif: structural and functional diversity. Protein Sci 5, 2375–2390.
Nishiki T, Augustine GJ (2004). Dual roles of the C2B domain of synaptotagmin I in synchronizing Ca^{2+}-dependent neurotransmitter release. J Neurosci 24, 8542–8550.
Nishizuka Y (1988). The molecular heterogeneity of protein kinase C and its implications for cellular regulation. Nature 334, 661–665.
Ohno S, Akita Y, Konno Y, Imajoh S, Suzuki K (1988). A novel phorbol ester receptor/protein kinase, nPKC, distantly related to the protein kinase C family. Cell 53, 731–741.
Ono Y, Fujii T, Ogita K, Kikkawa U, Igarashi K, Nishizuka Y (1988). The structure, expression, and properties of additional members of the protein kinase C family. J Biol Chem 263, 6927–6932.
Perin MS, Fried VA, Mignery GA, Jahn R, Südhof TC (1990). Phospholipid binding by a synaptic vesicle protein homologous to the regulatory region of protein kinase C. Nature 345, 260–263.
Radhakrishnan A, Stein A, Jahn R, Fasshauer D (2009). The Ca^{2+} affinity of synaptotagmin 1 is markedly increased by a specific interaction of its C2B domain with phosphatidylinositol 4,5-bisphosphate. J Biol Chem 284, 25749–25760.
Robinson IM, Ranjan R, Schwarz TL (2002). Synaptotagmins I and IV promote transmitter release independently of Ca^{2+} binding in the C(2)A domain. Nature 418, 336–340.
Rosenmund C, Stevens CF (1996). Definition of the readily releasable pool of vesicles at hippocampal synapses. Neuron 16, 1197–1207.
Schiavo G, Stenbeck G, Rothman JE, Sollner TH (1997). Binding of the synaptic vesicle v-SNARE, synaptotagmin, to the plasma membrane t-SNARE, SNAP-25, can explain docked vesicles at neurotoxin-treated synapses. Proc Natl Acad Sci USA 94, 997–1001.
Seven AB, Brewer KD, Shi L, Jiang QX, Rizo J (2013). Prevalent mechanism of membrane bridging by synaptotagmin-1. Proc Natl Acad Sci USA 110, E3243–E3252.
Stevens CF, Sullivan JM (2003). The synaptotagmin C2A domain is part of the calcium sensor controlling fast synaptic transmission. Neuron 39, 299–308.
Sutton RB, Davletov BA, Berghuis AM, Südhof TC, Sprang SR (1995). Structure of the first C2 domain of synaptotagmin I: a novel Ca^{2+}/phospholipid-binding fold. Cell 80, 929–938.
Sutton RB, Ernst JA, Brunger AT (1999). Crystal structure of the cytosolic C2A-C2B domains of synaptotagmin III. Implications for Ca^{2+}-independent snare complex interaction. J Cell Biol 147, 589–598.
Tucker WC, Chapman ER (2002). Role of synaptotagmin in Ca^{2+}-triggered exocytosis. Biochem J 366, 1–13.
Tucker WC, Weber T, Chapman ER (2004). Reconstitution of Ca^{2+}-regulated membrane fusion by synaptotagmin and SNAREs. Science 304, 435–438.
Ubach J, Zhang X, Shao X, Südhof TC, Rizo J (1998). Ca^{2+} binding to synaptotagmin: how many Ca^{2+} ions bind to the tip of a C2-domain? EMBO J 17, 3921–3930.
Vrljic M, Strop P, Ernst JA, Sutton RB, Chu S, Brunger AT (2010). Molecular mechanism of the synaptotagmin-SNARE interaction in Ca^{2+}-triggered vesicle fusion. Nat Struct Mol Biol 17, 325–331.
Wang P, Wang CT, Bai J, Jackson MB, Chapman ER (2003). Mutations in the effector binding loops in the C2A and C2B domains of synaptotagmin I disrupt exocytosis in a nonadditive manner. J Biol Chem 278, 47030–47037.
Zhang Z, Hui E, Chapman ER, Jackson MB (2010). Regulation of exocytosis and fusion pores by synaptotagmin-effector interactions. Mol Biol Cell 21, 2821–2831.
Zhang X, Kim-Miller MJ, Fukuda M, Kowalchyk JA, Martin TF (2002). Ca^{2+}-dependent synaptotagmin binding to SNAP-25 is essential for Ca^{2+}-triggered exocytosis. Neuron 34, 599–611.